Applied Physics Letters

Ultra-sensitive charge detection and latch memory using MoS_2-nanoresonator-based bifurcation amplifiers

Cite as: Appl. Phys. Lett. **118**, 053105 (2021); https://doi.org/10.1063/5.0031890
Submitted: 05 October 2020 . Accepted: 25 January 2021 . Published Online: 05 February 2021

Aneesh Dash, Swapnil K. More, Nishta Arora, and A. K. Naik

Applied Physics Letters ARTICLE scitation.org/journal/apl

Ultra-sensitive charge detection and latch memory using MoS_2-nanoresonator-based bifurcation amplifiers

Cite as: Appl. Phys. Lett. **118**, 053105 (2021); doi: 10.1063/5.0031890
Submitted: 5 October 2020 · Accepted: 25 January 2021 ·
Published Online: 5 February 2021

Aneesh Dash,[a] Swapnil K. More, Nishta Arora, and A. K. Naik[a]

AFFILIATIONS

Centre for Nano Science and Engineering, Indian Institute of Science, Bangalore 560012, India

[a]Authors to whom correspondence should be addressed: aneesh@iisc.ac.in and anaik@iisc.ac.in

ABSTRACT

Bifurcation amplifiers are known for their extremely high sensitivity to weak input signals. We implement a bifurcation amplifier by harnessing the Duffing nonlinearity in a parametrically excited MoS_2 nano-electromechanical system. We utilize the ultra-sensitive switching response between the two states of the bifurcation amplifier to detect as well as register charge-fluctuation events. We demonstrate open-loop real-time detection of ultra-low electrical charge perturbations of magnitude <10 e at room temperature. Furthermore, we show latching of the resonator onto one of the two states in response to short-lived charge fluctuations. These charge detectors offer advantages of room-temperature operation and tunable operation in the radio frequency regime, which could open several possibilities in quantum sensing.

Bifurcation amplifiers are promising candidates for ultra-sensitive detection of signals in quantum measurements.[1,2] These devices offer sharp step-like transitions in the output in response to minute changes in the input signal. Bifurcation amplifiers implemented using Josephson junctions are known to be useful in charge sensing and detection of superconducting qubits.[2–4] However, their implementation is limited to cryogenic temperatures. On the other hand, nanomechanical bifurcation amplifiers have readily achievable mechanical bifurcation points. These devices have the advantage of room-temperature operation and a simple device structure.[5–7] An implementation of a bifurcation amplifier using coupled nanomechanical resonators has shown exceptional charge sensitivity.[5] In a recent theoretical report, Takodaro *et al.* have proposed bifurcation amplifiers using nonlinear nanomechanical resonators as potential candidates for sensitive detection of digitally modulated force signals.[8] The operation of the devices in the nonlinear regime is crucial to the implementation of the bifurcation amplifiers. Nano-electromechanical systems (NEMS) based on layered materials, with tunable mechanical nonlinearities[9] at low amplitudes of vibration[10–16] and extraordinary sensitivity to external stimuli,[17–20] are well suited for the implementation of bifurcation amplifiers.[8]

In this work, we implement a parametrically excited bifurcation amplifier using an MoS_2 nano-resonator and demonstrate charge detection and memory with exquisite sensitivity. The bifurcation amplifier has step-like displacement-vs-excitation characteristics. At different operating frequencies, the tri-stable region of the bifurcation amplifier has different widths (hysteresis loops). At smaller widths, the device switches sharply between two states in response to small changes in excitation strength due to the accumulation of charges on the membrane. It is sensitive to both the increase and decrease in the accumulated charge and can respond to an electrical charge perturbation of about 130 e with a switching error probability less than 3×10^{-5}. This sensitivity is limited by the thermally activated inter-state transitions close to the critical point for the onset of nonlinearity. At larger widths of the tri-stable region, the device can operate as a latch memory, which can latch from one state to another in response to electrical charge less than 10 e. Thermally activated transitions in this regime are less due to larger activation energy required for inter-state transitions. The device remains latched to the vibration state even after the charge perturbation has vanished and can be reset only by turning the vibration off.

The device [shown in Fig. 1(a)] is a drum resonator fabricated using few-layer MoS_2 (details of fabrication are available in the supplementary material). The diameter of the drum is 3 μm. The circuit used for implementing the bifurcation amplifier is shown in Fig. 1(b). We use an electrical gate for capacitive actuation of the device, and the displacement is monitored by observing the change in capacitance.[10,15] The membrane acts as the moving plate of a parallel-plate capacitor,

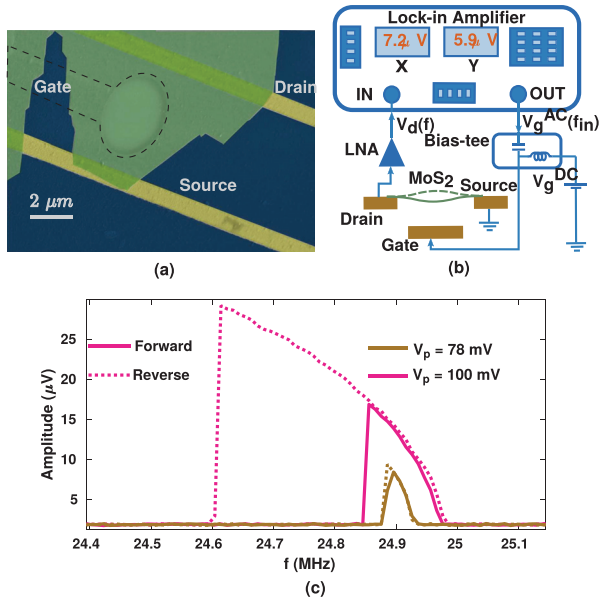

FIG. 1. (a) Scanning electron micro-graph (false-colored) of the MoS_2 drum resonator: the local gate (highlighted) is under the suspended membrane, (b) schematic of the circuit used for experimental measurements, and (c) forward and reverse traces of the amplitude responses of the parametrically excited resonator for $V_p = 78$ mV and $V_p = 100$ mV: the responses show negative effective Duffing nonlinearity.

with the gate as the stationary plate. The electrostatic force, due to the applied DC voltage (V_g^{DC}) at the gate, pulls the membrane down, producing a strain that tunes the resonant frequency of the device. An AC voltage signal [$V_g^{AC} = V_p \cos(2\pi f_{in} t)$] from a lock-in amplifier (LIA) is added to the DC voltage to produce a sinusoidal variation in the force acting on the membrane.[10] The detection of displacement is at frequency f, which is close to the resonant frequency f_0 of the resonator.

A directly driven resonator($f_{in} \approx f_0$) is limited by poor signal-to-noise ratio (SNR) and a non-ideal bifurcation response (see the supplementary material).[1,8,10,21] Hence, we use parametric excitation ($f_{in} \approx 2f_0$) to implement the bifurcation amplifier, whose displacement-vs-excitation response is expected to have near-ideal step-like characteristics.[21] In this scheme, the AC signal (parametric pump) modulates the strain in the vibrating membrane at twice the resonant frequency. This results in self-oscillation when the strength of the pump is sufficient to overcome the damping.[21,22] Parametric excitation offers further advantages of minimal electrical background in the measured displacement and higher amplitudes of vibration.[15,22–24] The results of forward (low to high) and reverse (high to low) frequency sweeps with parametric excitation ($V_p = 78$ mV and $V_p = 100$ mV) at $V_g^{DC} = 17$ V are shown in Fig. 1(c). The bending of the resonance toward lower frequencies (nonlinear frequency-softening) and the hysteresis on the low-frequency side are characteristic of a resonator with negative Duffing nonlinearity.[12,15] The hysteresis between the forward and reverse traces at $V_p = 78$ mV is minimal, indicating that the resonator is close to the critical point for the onset of Duffing nonlinearity. As V_p is increased to 100 mV, a large hysteresis between the forward and reverse sweeps is observed.

The density plots (forward and reverse frequency sweep) for parametric excitation at different values of V_p are shown in Figs. 2(a) and 2(b), respectively. The tongue-shaped responses are characteristic of parametric excitation.[15,21,23] The tongue of the forward sweep has smaller width than that of the reverse sweep due to negative effective Duffing nonlinearity in the resonator.[15] To realize the bifurcation amplifier, we operate the device at a fixed frequency [marked by dashed lines in Figs. 2(a) and 2(b)] and sweep the excitation strength (V_p) at twice the operating frequency. The amplitude responses for the forward (low to high) and reverse (high to low) sweeps of V_p at $f_{in} = 2 \times 24.89$ MHz $(2f_1)$ and $f_{in} = 2 \times 24.86$ MHz $(2f_2)$ are shown in Figs. 2(c) and 2(d), respectively. We use these step-like responses as bifurcation amplifiers.[21] The responses for the operating frequencies in between f_1 and f_2 are shown in the supplementary material.

Unlike the directly driven bifurcation amplifier, these parametric responses have an input-independent state 0 (no forced oscillation) when the pump is not strong enough to overcome the linear damping. Beyond a certain pump strength, the resonator switches to a stable vibration state 1. We note that the state 1 referred to here corresponds to two states with equal amplitude and opposite phases, which is the characteristic of parametrically excited resonance with a double-frequency pump.[25–27] In the tri-stable region, there are three stable states, state 0 as well as the two states 1.

In Fig. 2(c) ($f_{in} = 2f_1$), the width of the tri-stable region is minimal since the resonator is close to the critical point. The resonator switches between states 0 and 1 if the amplitude of the pump is modulated between the two sides of the step. This modulation is analogous to the accumulation of charge on the resonator and can be used to estimate the charge sensitivity. With minimal hysteresis, a small change in charge can switch the resonator between the two states. At $f_{in} = 2f_2$ [Fig. 2(d)], the step response has a wide tri-stable region. With the large hysteresis, the bifurcation amplifier can act as a sensitive latch memory for charges.

A change δV in the amplitude of the parametric pump causes a change $\delta Q = C_g \delta V$ in the charge accumulation on the resonator, where C_g is the gate capacitance (dielectric capacitance) of the device estimated with a parallel-plate approximation based on the geometry; $C_g = \epsilon_0 A/d \approx 0.7$ fF, $d = 300$ nm, and $A \approx 24\,\mu\text{m}^2$ (details are available in the supplementary material). The charge sensitivity of the bifurcation amplifier is measured by digitally modulating the pump amplitude (V_p) between the levels $\hat{V}_p - \delta V/2$ and $\hat{V}_p + \delta V/2$ [where $\hat{V}_p$ is the voltage set point shown in Figs. 2(c) and 2(d), respectively] and monitoring the output displacement amplitude of the device. The details about the implementation are given in the supplementary material. For $f_{in} = 2f_1$, the two voltage levels lie on either side of the step response, as shown in Fig. 3(a). The transition between the two states is due to an increase or decrease in charge, respectively. Figure 3(b) shows the time traces of the demodulated displacement amplitude of the device at different δQ for a square-wave modulation of V_p. As δQ is reduced, the switching error between states 1 and 0 increases. This is due to slow-timescale thermally activated transitions between the states close to the critical point, which are expected in parametrically excited systems.[26,28]

Figure 4(a) shows the demodulated amplitude of the device at computer-generated random values of V_p. We observe that the highlighted multi-valued region, where the device switches between states 1 and 0 on its own, is broader than the tri-stable region observed

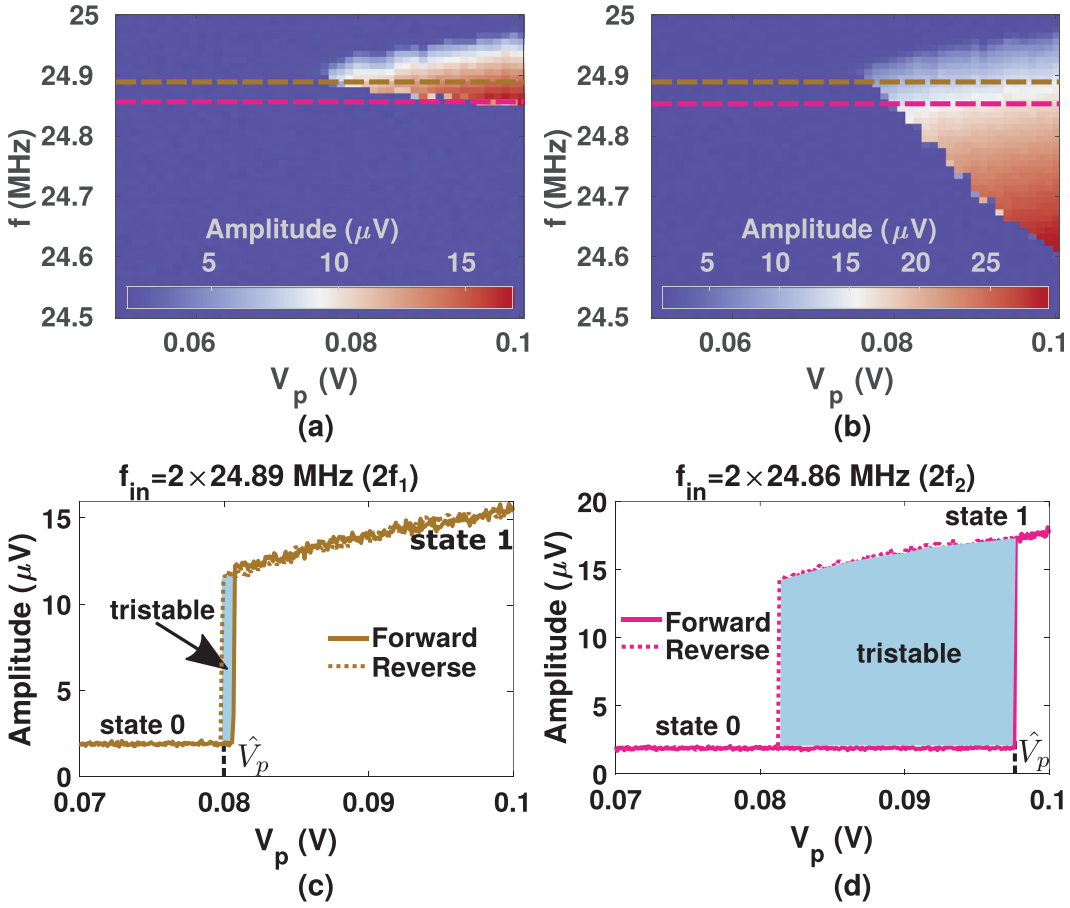

FIG. 2. [(a) and (b)] Characteristic tongue-shaped density plots for (a) forward and (b) reverse frequency sweeps ($f_{in} = 2f$) and [(c) and (d)] forward and reverse traces of the displacement amplitude of the resonator as a function of V_p at a fixed frequency (c) $f_{in} = 2 \times 24.89\,\text{MHz}\,(2f_1)$ and (d) $f_{in} = 2 \times 24.86\,\text{MHz}\,(2f_2)$ [along the dashed lines shown in (a) and (b)]: the tri-stable region is broader in (d).

in Fig. 2(c). For the continuous sweep [Fig. 2(c)], the time step between two consecutive inputs is less than 100 μs. On the other hand, the switching time/time step is much longer in Figs. 3(b) and 4(a). A longer measurement time allows for more of the slow thermally activated transitions to be recorded in the measurements.[5,26]

To get a statistical estimate of the switching error, we use a pseudorandom bit sequence (PRBS) of length $2^{15} - 1$ to digitally modulate the pump and count the number of instances of incorrect switching (state 0 instead of 1 or vice versa). The statistically estimated probability of switching error (P_{err}) as a function of δQ is shown in Fig. 4(b). P_{err} is observed to be greater than 10^{-3} below $\delta Q = 114\,\text{e}$ and decreases with the increase in δQ. At $\delta Q = 131\,\text{e}$ [highlighted point in Fig. 4(b)], we do not record any switching error for $2^{15} - 1$ bits ($P_{err} \leq 3 \times 10^{-5}$). The histogram of the demodulated amplitudes at this δQ, shown in the inset of Fig. 4(b), shows well-separated clusters of amplitude corresponding to states 1 and 0 and the boundary used for making an error decision. The measurement bandwidth used in these experiments is 625 Hz. Similar characterization of the switching error, performed on a second device, is given in the supplementary material.

We present a qualitative explanation of the room-temperature thermally activated state transitions following the theoretical understanding of similar transitions activated by quantum fluctuations (at low temperature) in such systems.[26] Figure 4(c) shows the outlines of the two density plots shown in Figs. 2(a) and 2(b), with the mono-stable, bi-stable, and tri-stable regions marked. The pairs of points $P_1^{tri,bi}$ and $P_2^{tri,bi}$ are the operating points for the transition from state 0 to state 1 for $f_{in} = 2f_1$ and $f_{in} = 2f_2$, respectively. The variation of the resonator potential with respect to displacement in the vicinity of these points is shown in Fig. 4(d). In the mono-stable region, the resonator has a harmonic potential with a single minimum at state 0 (stable). In the bi-stable region, state 0 is unstable (maximum) and only the two states 1 are stable (minima). In the tri-stable region, all the three states are stable (minima), while there are two unstable states marked as 1′. The pairs of points $P_1^{tri,bi}$ are close to the critical point P_c, which is at the intersection of all the three regions marked in Fig. 4(c). At P_c, the resonator-potential distribution almost resembles the harmonic potential of the mono-stable region. Hence, at $P_1^{tri,bi}$, the minima and maxima corresponding to states 1 and 1′ in the resonator potential are extremely shallow, as shown in Fig. 4(d). Therefore, a small thermal

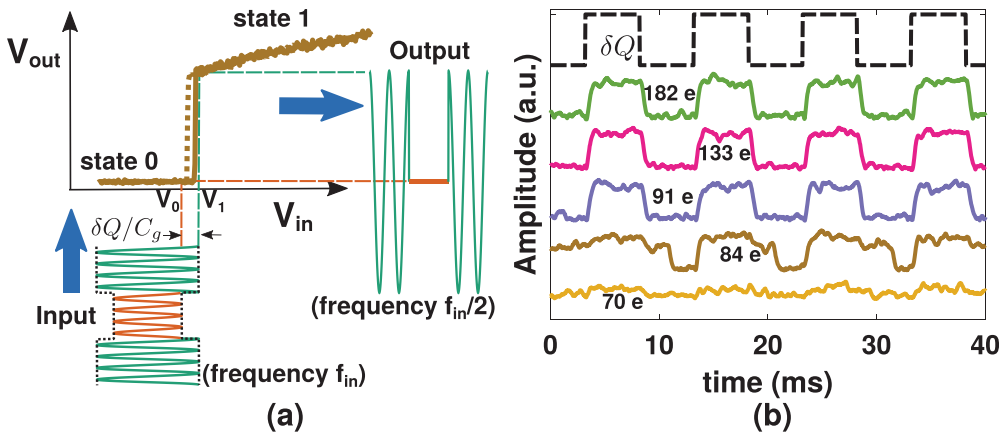

FIG. 3. (a) Schematic of the operation of the charge detector at $f_{in} = 2f_1$: a step change in charge produces a step change in the demodulated displacement amplitude. (b) Time traces (vertically offset for clarity) of the demodulated displacement amplitude at different values of δQ: switching error is observed at lower δQ.

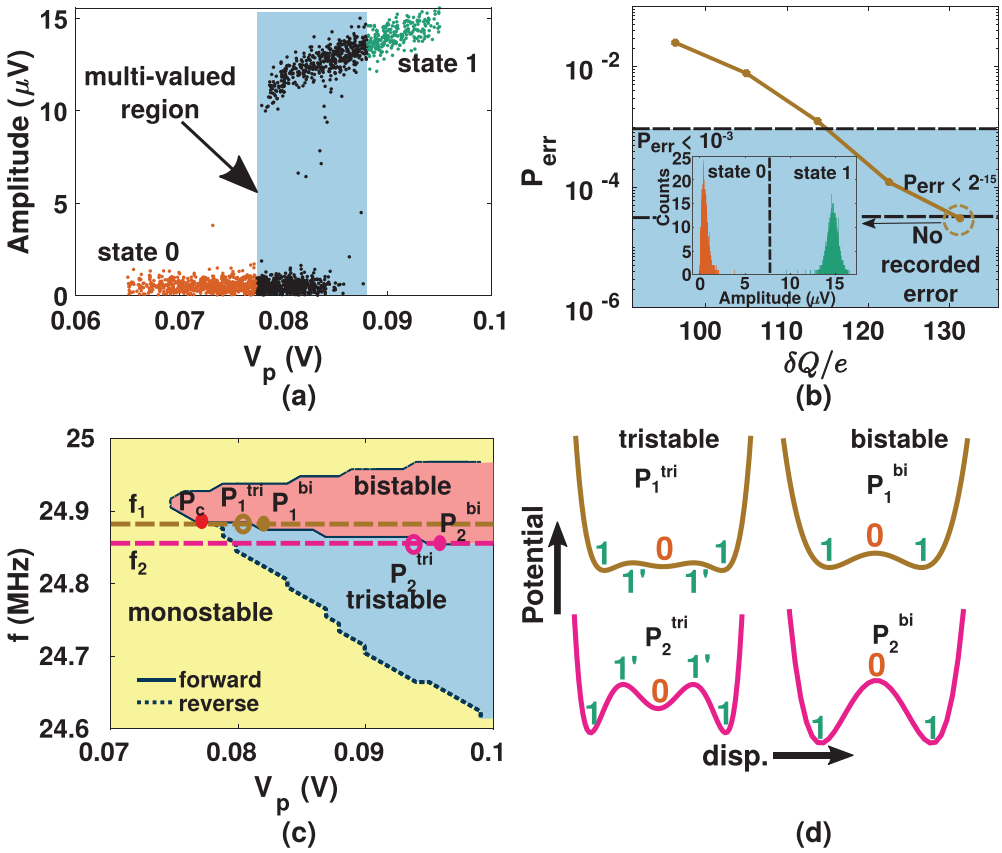

FIG. 4. (a) Amplitude response of the resonator at pseudo-random input voltages: the highlighted multi-valued region is broader than in Fig. 2(c); (b) probability of switching error of the bifurcation amplifier at different δQ: the inset shows the histogram of the occurrences of the demodulated amplitude at $\delta Q = 131\ e$; (c) outlines of the density plots [shown in Figs. 2(a) and 2(b)]: the mono-stable, bi-stable, tri-stable regions, the critical point P_c, and the pairs of points $P_1^{tri,bi}$ and $P_2^{tri,bi}$ corresponding to inter-state transitions at $f_{in} = 2f_1$ and $f_{in} = 2f_2$, respectively, are marked; and (d) schematic of the potential vs displacement curves for the tri-stable and the bi-stable regions in the vicinity of the points $P_1^{tri,bi}$ (shallow extrema) and $P_2^{tri,bi}$ (less shallow extrema).

activation energy at room temperature is sufficient to cause inter-state transitions, as is evident from the switching error.[26] However, when we move away from the critical point to the pair of points $P_2^{tri,bi}$, the resonator potential has larger energy barriers, making the thermally activated transitions less likely[26] and allowing smaller changes in electrical charge to be detected.

At $f_{in} = 2f_2$, the bifurcation amplifier has a broad tri-stable region, as shown in Fig. 2(d). When $\hat{V}_p$ is set close to the upward-jump boundary of the tri-stable region, the two voltage levels $V_1 = \hat{V}_p + \delta V/2$ and $V_0 = \hat{V}_p - \delta V/2$ are aligned to the step response as shown in Fig. 5(a). If the device is initially in state 0 and there is an increase in pump amplitude corresponding to δQ, the device switches to state 1. However, a decrease in pump amplitude does not switch the device back to state 0, due to the hysteresis in the amplitude response of the device, as shown in Fig. 5(a). Hence, the device remains latched to state 1 even if the charge signal is removed and acts like a charge-sensitive latch memory. Resetting the device to state 0 requires lowering the parametric excitation strength (V_p) until the resonator switches to state 0 (below 80 mV in this case). Figure 5(b) shows the time traces of the demodulated amplitude of the device at different values of δQ at a measurement bandwidth of 625 Hz. It must be noted that the step height corresponding to the transition and the SNR remain almost constant irrespective of the signal strength, since there are no observed vibrations in state 0 and the vibration amplitude is saturated in state 1.[29] Therefore, this device is a charge-event detector, which responds identically to the occurrence of any charge perturbation. The dashed line represents the input signal. It is observed that the latch memory is responsive to δQ as low as 9 e. We note, however, that as the magnitude of δQ is reduced, the probability of error is expected to be larger, similar to what is observed in Fig. 4(b).

Therefore, this implementation of the bifurcation amplifier can record short-lived charge signals with extraordinary sensitivity. Ultrasensitive electrometers used for quantum sensing, such as the RF single electron transistor and Josephson bifurcation amplifier, can detect single electrons and have noise-limited sensitivities on the order of $10^{-5}\ e/\sqrt{Hz}$.[2–4,30] However, their operating temperature is below 1 K. Micromechanical and nanomechanical resonators have been used to detect charges in the range of $70 - 100$ e at room temperature with sensitivities on the order of $10^{-1}\ e/\sqrt{Hz}$ and estimated low temperature sensitivities on the order of $10^{-5}\ e/\sqrt{Hz}$, limited by the thermal noise.[31–33] Nanomechanical bifurcation amplifiers based on GaAs nanoresonators have also shown similar charge detection capabilities.[5] With the MoS_2 nanoresonators, the minimum detected charge signal in real time at room temperature is less than 10 e, which is a significant improvement in mechanical electrometry. Lowering the temperature is expected to yield sensitivities similar to other nanomechanical electrometers. The summary of the performance metrics of different electrometers is shown in the supplementary material.

In conclusion, we have demonstrated bifurcation amplifiers, implemented using a parametrically excited nonlinear MoS_2 nanomechanical resonator, whose displacement amplitude is sensitive to charge. Close to the critical point for the onset of nonlinearity, the device can respond to charge signals of magnitude on the order of 100 e at room temperature, limited by the slow-timescale thermally activated state transitions. Away from the critical point, the device operates as a charge-sensitive latch memory, which switches its vibration state once in response to a change in charge and latches to that vibration state even after the charge is removed. This latch memory is found to be responsive to charges <10 e at room-temperature in open-loop operation. The SNR and height of the step responses shown in Figs. 3(b) and 5(b) remain almost constant at all δQ, making these devices sensitive charge-event detectors. The limit of detection imposed by room-temperature thermally activated transitions and fluctuations in the position of the bifurcation points [in Fig. 4(c)] requires further investigation. The room-temperature operation could be further improved using closed loop measurements.[34] Improved device structures with a compliant membrane and optimal separation between the membrane and the gate can lead to better room-temperature charge sensitivity. At low temperatures, better charge sensitivity is expected since the thermally activated transitions would be minimal and the device would be limited by inter-state transitions activated by quantum fluctuations.[2,26] The operating frequencies of these devices are on the order of 10 MHz and can be tuned with static

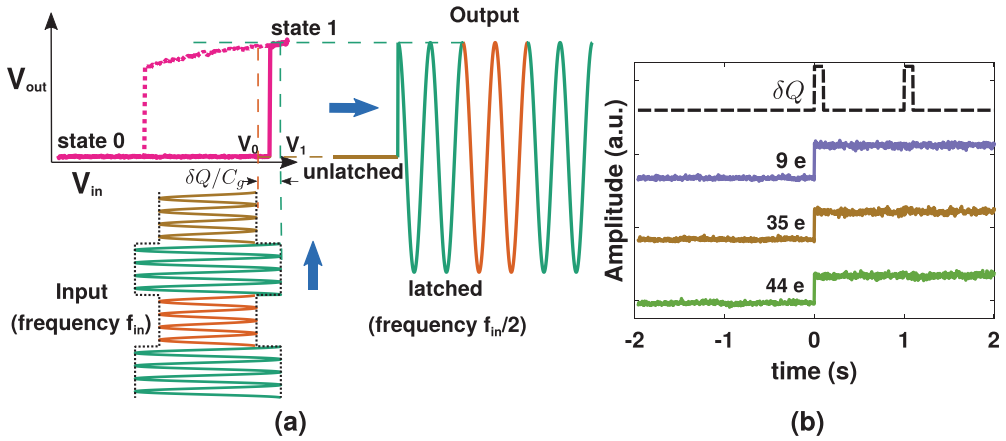

FIG. 5. (a) Schematic of the operation of the charge-sensitive latch memory at $f_{in} = 2f_2$: a step change in charge produces a step change in the demodulated displacement amplitude, which persists even after the charge is removed and can be reset only by turning the vibration off, and (b) time traces (vertically offset for clarity) of the demodulated amplitude of the bifurcation amplifier for different values of δQ: the latching operation for a minimum δQ of 9 e is observed at room temperature.

strain imposed at the clamps or through electrostatic pull by the gate electrode.[10,16] Using thinner membranes and smaller drum geometries can also help achieve higher resonant frequencies.[11] Furthermore, improved transduction mechanisms can help read out higher-order mechanical modes, which have higher resonant frequencies. These bifurcation amplifiers hold significant promise for quantum-sensing applications. The tunability of the resonant frequency of these devices in the radio frequency regime and tunable mechanical nonlinearities make them more versatile for these applications. Further investigation on the limitations of the charge sensitivity of the latch memory could open unexplored routes in nanomechanical sensing.

See the supplementary material for details of fabrication, data of the two devices, and details of the experimental setup.

We acknowledge financial support from the Science and Engineering Research Board, DST India through Grant No. EMR/2016/006479 and DST Nanomission, India through Grant No. SR/NM/NS-1157/2015(G). We also acknowledge funding from MHRD, MeitY and DST Nano Mission, for supporting the facilities at the Centre for Nano Science and Engineering. We thank Dr. Parmeshwar Prasad for performing the initial trials of parametric excitation on one of the devices. We also thank Professor Mark Dykman, Professor Shankar Kumar Selvaraja, and Mr. Avijit Chatterjee for helpful discussions.

There are no conflicts of interest to declare.

DATA AVAILABILITY

The data that support the findings of this study are available from the corresponding authors upon a reasonable request.

REFERENCES

[1]K. Wiesenfeld and B. Mcnamara, Phys. Rev. A **33**, 629 (1986).
[2]I. Siddiqi, R. Vijay, F. Pierre, C. M. Wilson, M. Metcalfe, C. Rigetti, L. Frunzio, and M. H. Devoret, Phys. Rev. Lett. **93**, 207002 (2004).
[3]I. Siddiqi, R. Vijay, F. Pierre, C. M. Wilson, L. Frunzio, M. Metcalfe, C. Rigetti, and M. H. Devoret, in *Quantum Computing in Solid State Systems*, edited by B. Ruggiero, P. Delsing, C. Granata, Y. Pashkin, and P. Silvestrini (Springer, New York, 2006), pp. 28–37.
[4]R. Vijay, M. H. Devoret, and I. Siddiqi, Rev. Sci. Instrum. **80**, 111101 (2009).
[5]R. B. Karabalin, R. Lifshitz, M. C. Cross, M. H. Matheny, S. C. Masmanidis, and M. L. Roukes, Phys. Rev. Lett. **106**, 094102 (2011).
[6]E. Buks and B. Yurke, Phys. Rev. E **74**, 046619 (2006).
[7]R. Almog, S. Zaitsev, O. Shtempluck, and E. Buks, Appl. Phys. Lett. **88**, 213509 (2006).
[8]Y. Tadokoro, H. Tanaka, and M. I. Dykman, Sci. Rep. **8**, 11284 (2018).
[9]C. Samanta, N. Arora, K. K. V, S. Raghavan, and A. K. Naik, Nanoscale **11**, 8394 (2019).
[10]C. Chen, S. Lee, V. V. Deshpande, G.-H. Lee, M. Lekas, K. Shepard, and J. Hone, Nat. Nanotechnol. **8**, 923 (2013).
[11]J. Lee, Z. Wang, K. He, R. Yang, J. Shan, and P. X.-L. Feng, Sci. Adv. **4**, eaao6653 (2018).
[12]C. Samanta, N. Arora, and A. K. Naik, Appl. Phys. Lett. **113**, 113101 (2018).
[13]C. Samanta, P. R. Y. Gangavarapu, and A. K. Naik, Appl. Phys. Lett. **107**, 173110 (2015).
[14]M. M. Parmar, P. R. Y. Gangavarapu, and A. K. Naik, Appl. Phys. Lett. **107**, 113108 (2015).
[15]P. Prasad, N. Arora, and A. K. Naik, Nanoscale **9**, 18299 (2017).
[16]C. Chen, "Graphene nanoelectromechanical resonators and oscillators," Ph.D. thesis (Columbia University, 2013).
[17]J. Chaste, A. Eichler, J. Moser, G. Ceballos, R. Rurali, and A. Bachtold, Nat. Nanotechnol. **7**, 301 (2012).
[18]A. K. Naik, M. S. Hanay, W. K. Hiebert, X. L. Feng, and M. L. Roukes, Nat. Nanotechnol. **4**, 445 (2009).
[19]J. S. Bunch, A. M. van der Zande, S. S. Verbridge, I. W. Frank, D. M. Tanenbaum, J. M. Parpia, H. G. Craighead, and P. L. McEuen, Science **315**, 490 (2007).
[20]P. Weber, J. Güttinger, A. Noury, J. Vergara-Cruz, and A. Bachtold, Nat. Commun. **7**, 12496 (2016).
[21]A. H. Nayfeh and D. T. Mook, in *Nonlinear Oscillations* (Wiley-VCH Verlag GmbH, 1995), pp. 161–257.
[22]D. Rugar and P. Grütter, Phys. Rev. Lett. **67**, 699 (1991).
[23]A. Eichler, J. Chaste, J. Moser, and A. Bachtold, Nano Lett. **11**, 2699 (2011).
[24]J. P. Mathew, R. N. Patel, A. Borah, R. Vijay, and M. M. Deshmukh, Nat. Nanotechnol. **11**, 747 (2016).
[25]I. Mahboob and H. Yamaguchi, Nat. Nanotechnol. **3**, 275 (2008).
[26]Z. R. Lin, Y. Nakamura, and M. I. Dykman, Phys. Rev. E **92**, 022105 (2015).
[27]C. M. Wilson, T. Duty, M. Sandberg, F. Persson, V. Shumeiko, and P. Delsing, Phys. Rev. Lett. **105**, 233907 (2010).
[28]H. Kramers, Physica **7**, 284 (1940).
[29]R. Lifshitz and M. C. Cross, "Nonlinear dynamics of nanomechanical and micromechanical resonators," in *Reviews of Nonlinear Dynamics and Complexity* (John Wiley and Sons, Ltd, 2009), Chap. 1, pp. 1–52, see https://onlinelibrary.wiley.com/doi/pdf/10.1002/9783527626359.ch1.
[30]R. J. Schoelkopf, P. Wahlgren, A. A. Kozhevnikov, P. Delsing, and D. E. Prober, Science **280**, 1238 (1998).
[31]D. Chen, H. Zhang, J. Sun, M. Pandit, G. Sobreviela, Y. Wang, Q. Zhang, X. Chen, A. Seshia, and J. Xie, Phys. Rev. Appl. **14**, 014001 (2020).
[32]A. N. Cleland and M. L. Roukes, Nature **392**, 160 (1998).
[33]X. Wang, D. Pu, R. Huan, X. Wei, and W. Zhu, "Ultrasensitive charge detection utilizing coupled nonlinear micromechanical resonators," arXiv:1907.08394 (2019).
[34]M. Yuksel, E. Orhan, C. Yanik, A. B. Ari, A. Demir, and M. S. Hanay, Nano Lett. **19**, 3583 (2019).